Research paper

Stress Wave Tomography for the Quantification of Artificial Hole Detection in Camphor Trees (*Cinnamomum camphora*)

Cheng-Jung Lin,[1,6] Tun-Tschu Chang,[2] Ming-Yang Juan,[2]
Ta-Te Lin,[3] Chia-Lin Tseng,[4] Ya-Nan Wang,[5] Ming-Jer Tsai[5]

【Summary】

The purpose of this study was to evaluate defects/holes in trees using a stress wave tomographic technique. Results revealed that there was a significant positive relationship of the residual disc diameter ratio with the stress wave velocity, and a negative relationship with a reduction in the corresponding stress wave velocity in the virtual radial direction. A difference in the mapped color and stress wave velocity between the hole area and its surrounding sound area was obvious, and when the ratio of the hole area to the cross-sectional area exceeded 2.3%, the hole was detectable by tomography. A significant positive relationship between wood density and stress wave velocity of the transverse section was found in this study. Moreover, above the fiber saturation point, stress wave velocities tended to decrease with increasing moisture contents using tomography. Experimental results could provide some vital information for detecting defect locations and sizes in trunk cross-sections.

Key words: stress wave, tomographic technique, nondestructive evaluation, *Cinnamomum camphora*.

Lin CJ, Chang TT, Juan MY, Lin TT, Tseng CL, Wang YN, Tsai MJ. 2011. Stress wave tomography for the quantification of artificial hole detection in camphor trees (*Cinnamomum camphora*). Taiwan J For Sci 26(1):17-32.

[1] Forest Utilization Division, Taiwan Forestry Research Institute, 53 Nanhai Rd., Taipei 10066, Taiwan. 林業試驗所森林利用組，10066台北市南海路53號。

[2] Forest Protection Division, Taiwan Forestry Research Institute, 53 Nanhai Rd., Taipei 10066, Taiwan. 林業試驗所森林保護組，10066台北市南海路53號。

[3] Department of Bio-Industrial Mechatronics Engineering, National Taiwan Univ., 1 Roosevelt Rd., Sec. 4, Taipei 10617, Taiwan. 國立台灣大學生物產業機電工程學系，10617台北市羅斯福路四段1號。

[4] The Experimental Forest, College of Bioresources and Agriculture, National Taiwan Univ., 12 Qianshan Rd., Sec. 1, Zhushan Township, Nantou 55750, Taiwan. 國立台灣大學生物資源暨農學院實驗林管理處，55750南投縣竹山鎮前山路一段12號。

[5] School of Forestry and Resource Conservation, National Taiwan Univ., 1 Roosevelt Rd., Sec. 4, Taipei 10617, Taiwan. 國立台灣大學森林環境暨資源學系，10617台北市羅斯福路四段1號。

[6] Corresponding author, e-mail:d88625002@yahoo.com.tw 通訊作者。

Received July 2010, Accepted September 2010. 2010年7月送審 2010年9月通過。

研究報告

應用波斷層影像技術定量評估樟樹人造孔洞之研究

林振榮[1,6] 張東柱[2] 阮名揚[2] 林達德[3] 曾家琳[4] 王亞男[5] 蔡明哲[5]

摘 要

本研究的目的是應用應力波斷層影像技術評估樟樹圓盤在不同大小的人造孔洞的影像反應，評估非破壞性參數與孔洞大小的關係，以瞭解非破壞性技術檢測孔洞的準確性，結果顯示徑向應力波速度與殘餘圓盤直徑比率之間有顯著的正相關性存在，而徑向應力波速度與相對應力波速度降低率之間有顯著的負相關性存在，當人造孔洞面積佔有圓盤橫斷面面積2.3%以上時，解析出的二維斷層影像圖中之孔洞及健全材質位置可以明顯的區別，因此，斷層影像法可以檢測樹木中的孔洞大小及相對位置，將圓盤橫斷面切成不同小區塊，其木材密度與影像解析的橫向應力波速度之間有顯著的正相關性存在，檢測不同含水率對應力波速度的影響，在纖維飽和點以上時應力波速度隨著含水率的增加而有降低的傾向，由斷層影像解析實驗的結果可以提供現場樹木橫斷面二維斷層影像解析的重要資訊。

關鍵詞：應力波、斷層影像技術、非破壞性評估、樟樹。

林振榮、張東柱、阮名揚、林達德、曾家琳、王亞男、蔡明哲。2011。應用波斷層影像技術定量評估樟樹人造孔洞之研究。台灣林業科學26(1):17-32。

INTRODUCTION

Effectively detecting deterioration due to decay and holes in trees is an important issue for the health and security of tree management. Various nondestructive evaluation (NDE) techniques are used to detect deterioration in trees in order to identify hazardous trees. Stress and ultrasonic wave transmission times or attenuation in wood have proven to be effective parameters for detecting and estimating deterioration in tree stems and wood structural members (Hoyle and Pellerin 1978, Mattheck and Bethge 1993, Ross and Pellerin 1994, Schad et al. 1996, Yamamoto et al. 1998, Lin et al. 2000). However, the 1-dimensional (1D) transmission wave test provides limited information about defects in trees. Reliable defect evaluation for imaging internal characteristics in logs and trees is possible by x-ray and neutron radiography, computed tomography, and magnetic resonance (Bethge et al. 1996, Bucur 2003, Nicolotti et al. 2003). These techniques can provide tomographic spatial locations of various defects and internal wood characteristics, but their application to trees has not been completely adopted because of the high costs, fear of x-rays and gamma rays, strong regulations, and the control of radiation sources associated with their use.

Some NDE techniques were recently developed for tomographic investigations. Tomography allows the reconstruction of a cross-section through an object by means of measurements performed on the object's surface and by measuring the energy that passes through the object itself (Stewart 1991). Currently, there is increasing interest in developing and using cost-effective technologies to evaluate and display 2D tomographic images of transverse sections of standing trees.

Acoustic tomographic measurements in wood have proven to be effective variables for detecting and estimating deterioration in different tree stems (Gilbert and Smiley 2004, Wang et al. 2007, 2009, Deflorio et al. 2008, Wang and Allison 2008). Sounding a tree by striking it with a tool can be used to detect advanced decay or hollows inside the trunk (McCracken 1985).

Ultrasonic tomography was applied by Tomikawa et al. (1990) and Biagi et al. (1994) to investigate poles and timber and by Comino et al. (2000) on living trees; Rust and Göcke (2000) applied sonic tomography to trees. Ultrasonic tomography allows the user to reconstruct the distribution of the ultrasonic wave velocity as it propagates within the investigated section. Because the wave velocity is related to the wood density and Young's modulus, a decreased velocity could, for instance, be diagnostic of fungal degradation of cell walls (Bucur 1995). The ultrasonic velocity was demonstrated to be very sensitive in the early stage of wood degradation (Wilcox 1988, Bauer et al. 1991). Furthermore, visual tree assessments are successfully supported by sound wave-based evaluations. Although acoustic tomography was proven to be the most-effective technique for detecting internal decay, to locate the position of defects, and estimate their sizes, shapes, and characteristics, tomography must be verified by corresponding cross-section inspection to understand the relationships between NDE characteristics and defects.

An ultrasonic tomographic technique was used to investigate standing tree cross-sections to detect the location and size of defects in Japanese cedar (softwood) (Lin et al. 2008). However, 1-by-1 measurements detected by 2 ultrasonic probes are inconvenient and we wanted to understand detection of defect efficiency by a stress wave tomographic technique in hardwood trees.

Therefore, the purpose of this study was to investigate the location and area of a artificial hole in camphor trees (*Cinnamomum camphora*) using the Arbotom stress wave system (Rinntech, German). The interrelationships among the residual disc diameter ratio, the ratio of the defect to disc area (tree defect parameters), the stress wave velocity, and the reduction in the corresponding stress wave velocity (NDE parameters) were examined and analyzed.

MATERIALS AND METHODS

Test materials

Four circular cross-sectional discs (350~400 mm in diameter and 100 mm thick) of visually solid and air-dried camphor tree (*C. camphora*) were prepared for this study. To prevent the occurrence of cracks during the drying process, the test discs were kept > 30% of moisture content. Multiple stress wave measurements were performed after chiseling a circular hole (an artificial defect) in the specimens. The shapes and sizes of the chiseled holes were divided into 2 kinds as shown in Fig. 1. For discs chiseled in the central area, a circular hole was gradually enlarged with a chisel from 0 to 240 mm in diameter at intervals of 30 mm. For discs chiseled in the side area, a circular hole was gradually enlarged with a chisel in the center of a quarter-divided disc from 0 to 120 mm in diameter at intervals of 30 mm.

Stress wave tomography

The stress wave equipment used for data acquisition was an Arbotom system. An electric signal is transformed by the transmitter probe into a stress wave pulse that travels through the wood, is received by the receiver probe, and is again transformed into an electric signal which

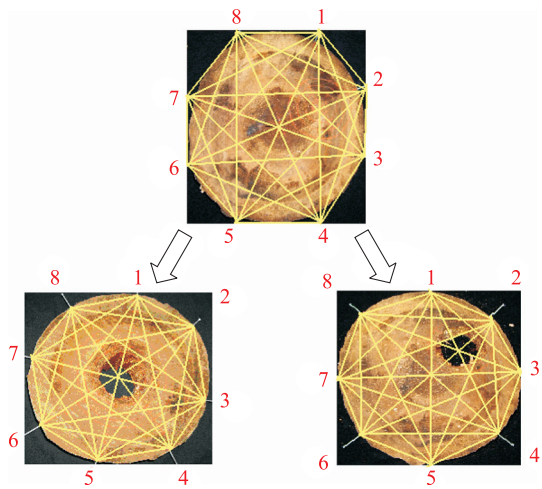

Fig. 1. Eight equidistant stress wave test points and 56 independent travel time measurements for each investigated section after a hole was chiseled in the central or side area. The stress wave probe was sequentially located at points 1, 2, 3, 4, 5, 6, 7, and 8. Upper, No-defect disc to the naked eye. Lower, Disc with an artificial hole. (a) A hole was chiseled in the central area of a trunk cross-section.

can be properly amplified and visualized, allowing for travel time measurements. The multiple stress wave measurements on the wood discs were carried out at 8 equidistant points. Specially made stainless-steel nails were driven into the xylem of each sample disc (Fig. 1). There was an angle of 90° between the nails and the trunk axis to connect the probes to detect the propagated stress wave. The transmitter probe was located at point 1 (one), and the wave pulse was acquired by the receiver probe at all other 7 points, then the transmitter was moved to point 2 (another). The measurements were repeated for all other positions of the probes, allowing for 56 (for a full round trip) independent propagation time measurements for each investigated section from Arbotom 2D software. Some important parameters such as cross-section form, species, corresponding position, and others, must be input into the software to establish corresponding measurements.

Evaluation parameters

According to the positions of all 8 measured stress wave test points, 4 types of stress wave travel routes in the discs were first divided into path A (2 measured points adjacent to each other, such as from points 1 to 2), path B (with a 1-point interval between 2 measured points, such as from points 1 to 3, 90° direction), path C (with a 2-point interval between 2 measured points, such as from points 1 to 4), and path D (virtual radial [180°] direction, with a 3-point interval between 2 measured points, such as from points 1 to 5) (Table 1, see figures).

The stress wave velocity (V), residual disc diameter ratio (RR), reduction in the corresponding stress wave velocity (RVD), stress wave velocity ratio along the paths D to B directions (RV), run time ratio along the paths B to D directions (RT), the ratio of the hole to the disc (HD), and the ratio of the hole to the disc diameter (RH) were estimated and calcu-

Table 1. Coefficients of linear regression formulae (Y = AX + B) for the relationship between the residual disc diameter ratio (X) and stress wave velocity (Y) of paths A, B, C, and D

Path	Regression equations	r^2	*F* value
Path A	Y = 32.28X + 708.0	0.28	2.77^{-}
Path B	Y = 150.29X + 747.6	0.78	24.3**
Path C	Y = 284.43X + 644.6	0.93	91.2**
Path D	Y = 376.72X + 551.2	0.96	167.8**

r^2, Coefficient of determination; $^{-} \geq 0.05$; ** $p < 0.01$.

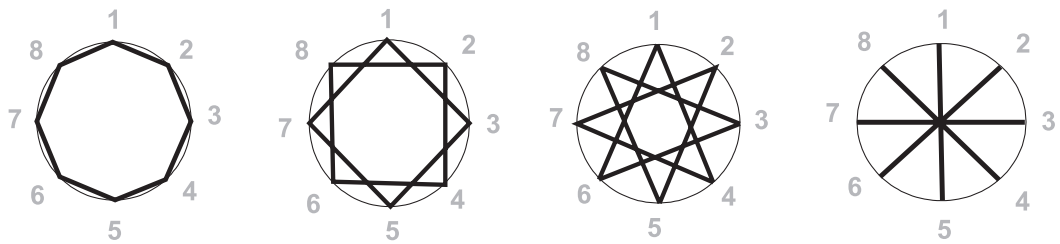

Path A Path B Path C Path D

Path A, 2 measured points adjacent to each other; path B, a 1-point interval between 2 measured points; path C, a 2-point interval between 2 measured points; path D, a 3-point interval between 2 measured points.

lated by the following formulae:

$$V = S/t, \quad [1]$$

$$RR = (D - d)/D, \quad [2]$$

$$RVD\ (\%) = 100 \times (V_{reference} - V_{measured})/V_{reference}, \quad [3]$$

$$RV = V_{Path\ D}/V_{Path\ B}, \quad [4]$$

$$RT = T_{Path\ B}/T_{Path\ D}, \quad [5]$$

$$HD = \pi(d/2)^2/\pi(D/2)^2, \quad [6]$$

$$RH = \text{hole diameter}/\text{disc diameter}; \quad [7]$$

where S is the distance between the 2 transducers, t is the run time of the pulse from the transmitting to the receiving probes, D is the disc diameter, d is the hole diameter, $V_{reference}$ is the stress wave velocity between probes before chiseling, $V_{measured}$ is the stress wave velocity between probes after chiseling, $V_{Path\ D}$ is the stress wave velocity obtained from path D (for codes, see Table 1), $V_{Path\ B}$ is the stress wave velocity obtained from path B, $T_{Path\ D}$ is the run time obtained from path D, and $T_{Path\ B}$ is the run time obtained from path B.

Conversion of the color image to gray-scale and stress wave velocity values

In order to evaluate the location and size of tree defects, 2D image tomographic software (Arbotom® software) developed by Rinntech (Heidelberg, Germany) was used. Tree defect tomograms in different colors, indicating various stress wave velocities, obtained from the Arbotom® software, could be converted into 256 gray shades. The Arbotom® software uses a 2-step filter to select the best values from the measurements to provide the optimum quality.

Values in the tomogram are weighted in contrast to values in the velocity table resulting from stress wave velocity measurements in this experiment. The Arbotom® software takes differences of radial and tangential velocities into account and standardizes them. In the surface graph, values are additionally weighted by parameters affected by tree spe-

cies (Anonymous 2005). The stress wave velocity at each pixel of the tomogram could be further calculated by the custom-made software developed in this study using Borland C++ builder (Borland, Texas, USA). Finally, the tomogram file was exported to Microsoft Excel (Redmond, CA, USA) for further assessment as shown in Fig. 2.

In order to understand the relationship between the wood density and stress wave velocity in a disc, small-dimension specimens (30×50×60 mm) were cut from 1 visually solid camphor tree disc after detecting 2D tomography images by the Arbotom system. The wood density and stress wave velocity of the small specimen from the corresponding position of the 2D tomographic image were calculated and estimated. Furthermore, the relationship between the wood density and stress wave velocity was examined.

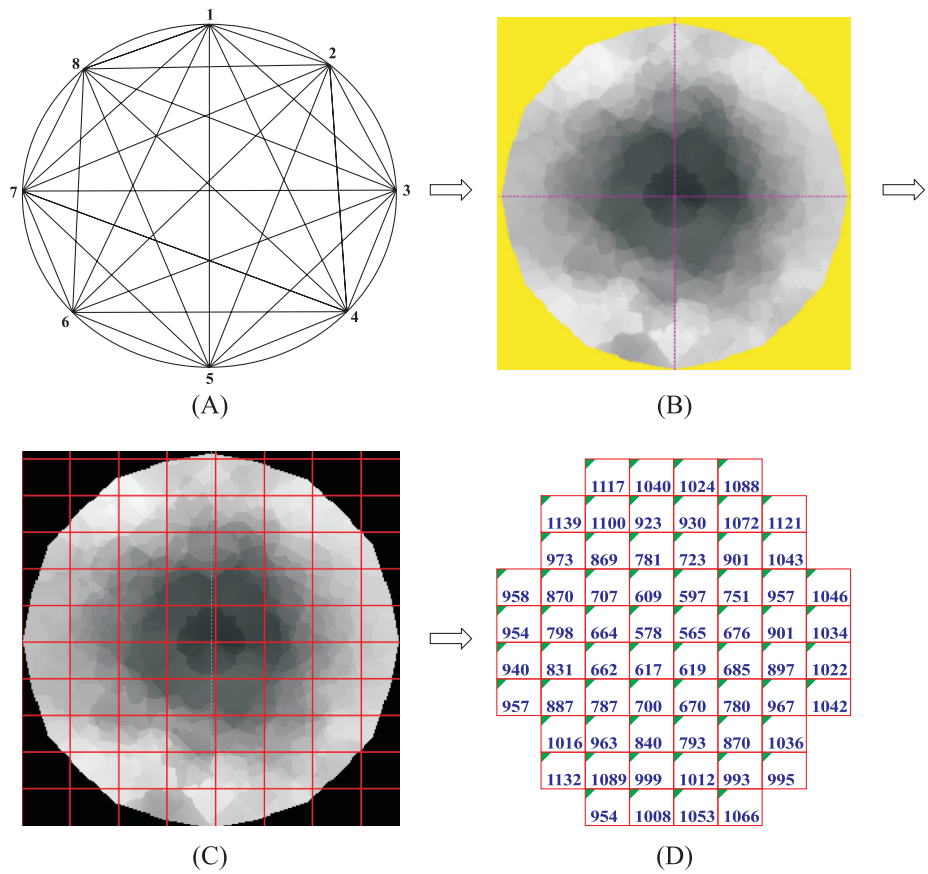

Fig. 2. Transfer procedure (from A to D) of the defect evaluation of a disc by the stress wave tomographic technique. (A) A 2D tomogram of the defect evaluation of a disc by a stress wave investigation (12 probs). (B) Conversion of the 2D image (A) into 256 gray shades with the Arbotom® software (Rinn Tech, Germany). (C) The stress wave velocity at each pixel of the tomogram calculated by the custom-made software developed in this study using Borland C++ builder. (D) Tomogram file exported to Microsoft Excel for further assessment (with the stress wave velocity calculated for each block).

In order to evaluate the relationship between the stress wave velocity and moisture content (MC) of various MC stages, 1 disc of a visually solid camphor tree was soaked in water for 3 mo to bring it above the fiber saturation point (FSP). The moisture content of the disc reached an average of about 90% (state of simulated live tree), and then we measured the stress wave velocity at different water stages.

The stress wave propagating through the disc in 2D was measured and recorded each time a weight loss of about 100~150 g occurred from the high green moisture content to near the FSP stage. The stress wave velocity was measured by the above-described methods, and the moisture content was calculated as follows:

$$MCu(\%) = (Wu - Wo)/Wo \times 100\%; \quad [8]$$

where MCu(%) is the MC of the test disc at various test stages, Wu is the weight of the test disc at various test stages, and Wo is the weight of the oven-dried disc.

RESULTS AND DISCUSSION

Effects of the residual disc diameter ratio on the stress wave velocity

Relationships between the stress wave velocity (round trip, paths A, B, C, and D) and residual disc diameter ratio are shown in Table 1. The highest coefficient of determination was found between the residual disc diameter ratio and the stress wave velocity along path D, with an r^2 value of about 0.96, followed in order according to the r^2 values (0.28~0.93) by paths C, B, and A. For paths A and B, the stress wave velocity was not influenced when the residual disc diameter ratio was more than about 0.3 and 0.6 according to the linear path of regression model analysis, respectively. Compared to paths A and B, the multiple measurements of the stress wave velocity along paths C and D were more feasible for detecting defects in the discs. This is because the stress wave travel route in wood is the fastest one, not the shortest one. Moreover, the stress wave velocity in the virtual radial direction was faster than that in the virtual tangential direction.

Ross and Pellerin (1994) indicated that the velocity in the radial direction was higher than that in the tangential direction. In the near tangential direction, such as path B, the propagation of the stress wave declines toward the receiver probe. As a result, the stress wave velocity was lower, even though there was no hole (defect) in the wood.

In this study, a change in the stress wave velocity along paths C and D was observed when the residual disc diameter ratio was 0.93 (i.e., a hole diameter of 30 mm). The reason is that a small hole diameter influenced paths C and D. In this experiment, velocity changes of paths A, B, C, and D were about 100~170 m s^{-1}. Comparing the obtained velocity change with the velocity determination error, it was found that the velocity change was smaller than 2-times the velocity determination error. This was in accordance with a previous report (Lin et al. 2008) for detecting defects in Japanese cedar trees using an ultrasonic tomographic technique.

Effects of the residual disc diameter ratio on reductions in the corresponding stress wave velocity

Relationships between reductions in the corresponding stress wave velocity and the residual disc diameter ratio are shown in Fig. 3. Two linear regression models were found between the residual disc diameter ratio and the reduction in the corresponding stress wave velocity along paths A and B. The intersecting points of the 2 regression equations were about 0.73 (path A) and 0.76 (path B).

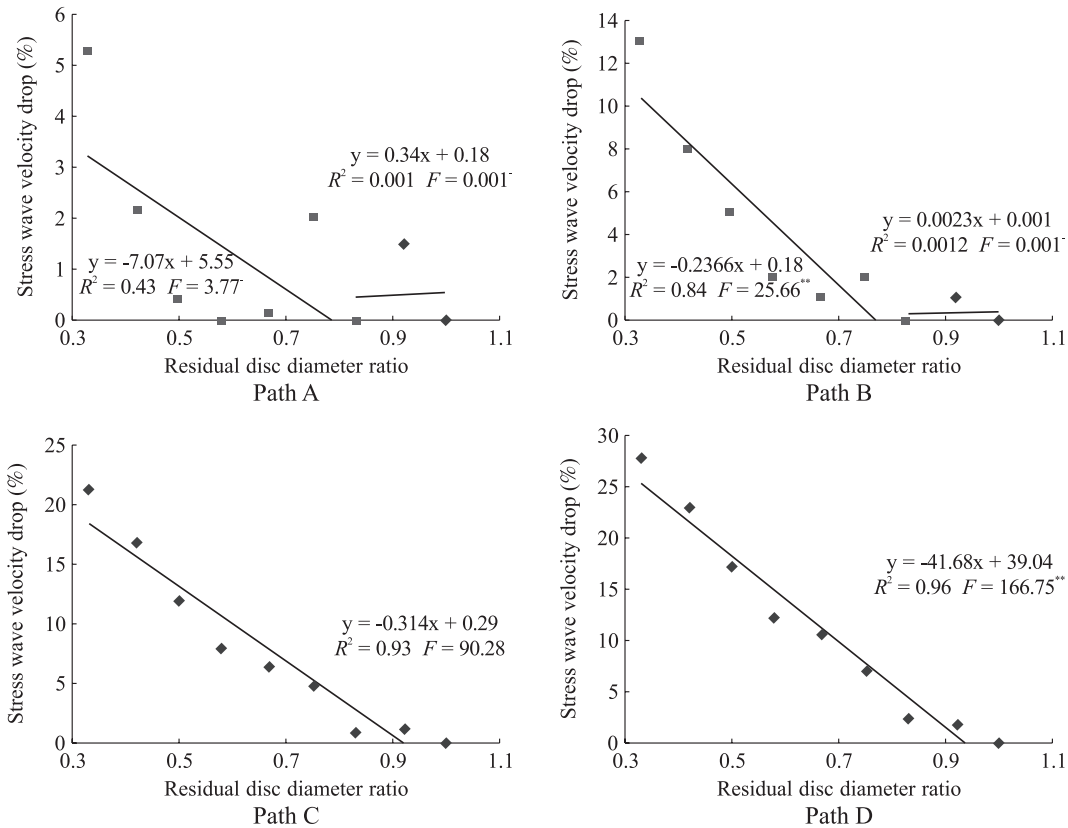

Fig. 3. Relationships between the residual disc diameter ratio and the corresponding stress wave velocity reduction (%) of paths A, B, C, and D in the central section area. For descriptions of paths A, B, C, and D, see Table 1.

This suggests that the reduction in the corresponding stress wave velocity was significantly influenced on paths A and B when the residual disc diameter ratios were < 0.73 and 0.76, respectively.

In this study, strong correlations between reductions in the corresponding stress wave velocity and residual disc diameter ratio were observed on paths C and D, with r^2 values of 0.93 and 0.96, respectively. This observation of strong correlations allowed us to conclude that the reduction in the corresponding stress wave velocity along paths C and D was a better method for evaluating defects occurring in the central area of a tree section.

Relationships between the stress wave travel time ratio along the path B to path D ($T_{Path\ B}/T_{Path\ D}$) and tree defect parameters

Table 2 reveals the correlations between the stress wave travel time ratio along paths B to D ($T_{Path\ B}/T_{Path\ D}$), the ratio of the hole to disc diameter (RH), the residual disc diameter ratio (RR), and the ratio of the hole to disc area (HD) area, analyzed by linear regression (Y = AX + B) formulae for detecting a defect in the central section area. These results were significant at the 0.01 confidence level, and the r^2 values of the regression analysis were 0.91~0.96. The $T_{Path\ B}/T_{Path\ D}$ values of the no-hole disc were 0.62~0.74.

Table 2. Correlations among the stress wave travel time ratio in paths B to D ($T_{Path\ B}/T_{Path\ D}$), the ratio of the hole to disc diameter (RH), the residual disc diameter ratio (RR), and the ratio of the hole to disc area (HD), as analyzed by linear regression (Y = AX + B) formulae for detecting a defect in the central section

Y	X	Regression equations	r^2	*F* value
$T_{Path\ B}/T_{Path\ D}$	RH	Y = -0.19X + 0.748	0.96	181.4**
	RR	Y = 0.189X + 0.558	0.96	170.1**
	HD	Y = -0.269X + 0.727	0.91	68.7**

** Significant difference at $p < 0.01$.

Huang et al. (1997) reported that $T_{Path\ B}/T_{Path\ D}$ values of non-decayed *Casuarina equisetifolia* trees were 0.76~0.83. However, those of decayed standing trees were 0.38~0.54. Lin et al. (2000) indicated that $T_{Path\ B}/T_{Path\ D}$ values of normal *Cunninghamia lanceolata* var. *konishii* trees were 0.91~0.95. However, those of various decayed standing trees were 0.21~0.82.

Effects of the ratio of the stress wave velocity along paths D to B on the hole area and position

Relationships between the ratio of stress wave velocity along paths D to B ($V_{Path\ D}/V_{Path\ B}$) and the ratio of the hole to disc area, analyzed by linear regression (Y = AX + B) formulae for a defect in the central area are shown in Table 3. $V_{Path\ D}/V_{Path\ B}$ values decreased with an increasing ratio of the hole to disc area. The relationships can be represented by negative linear regression formulae, and it was found that the coefficient of determination (r^2) values were 0.74~0.97. The $V_{path\ D}$ value (virtual radial) decreased with an increasing hole diameter, however, the $V_{path\ B}$ (virtual tangential) remained almost constant (in the center hole state). This suggests that the $V_{Path\ D}/V_{Path\ B}$ ratio can be used as an index for assessing the defect position and dimension in trees in this study.

When the defect was in the side area, $V_{Path\ D}/V_{Path\ B}$ values became more diverse as the ratio of the hole to disc area increased. However, experimental results found that the values of $V_{1\sim5}/V_{2\sim8}$ and $V_{3\sim7}/V_{2\sim4}$ increased with an increasing ratio of the hole to disc area. The relationships can be represented by positive linear regression formulae (r^2 = 0.92 and 0.99). On the contrary, values of $V_{2\sim6}/V_{1\sim3}$ and $V_{6\sim2}/V_{5\sim7}$ decreased with increasing hole/section area ratios. The relationships can be represented by negative linear regression formulae (r^2 = 0.99 and 0.94). Relationships between the 4 directional $V_{Path\ D}/V_{Path\ B}$ values and the ratios of the hole to disc area for defect detection in the side area are plotted in Fig. 4. This means that the stress wave velocity decreased when the stress wave propagation route approached a defect in a tree section. Therefore, these evaluation parameters ($V_{1\sim5}/V_{2\sim8}$, $V_{3\sim7}/V_{2\sim4}$, $V_{2\sim6}/V_{1\sim3}$, and $V_{6\sim2}/V_{5\sim7}$) can be used as an index for assessing the defect position in transverse sections of trees. Lin et al. (2008) also indicated that these evaluation parameters can be used as an index for assessing the defect position in Japanese cedar trees by an ultrasonic technique.

Relationships among stress wave velocities obtained from stress wave tomography, the ratio of the hole to disc diameter, the residual disc diameter ratio, and the ratio of the hole to disc area

Table 3. Correlations between the stress wave velocity along the paths D to B ($V_{Path\ D}/V_{Path\ B}$) and the ratio of the hole to disc area (HD), analyzed by linear regression formulae (Y = AX + B) for detecting a hole in the central section

X	Y	A	B	r^2	*F* values
HD	V1~5/V2~8	-0.26	1.14	0.88	80.52**
	V2~6/V1~3	-0.52	0.91	0.90	61.67**
	V3~7/V2~4	-0.60	1.21	0.93	77.19**
	V4~8/V3~5	-0.19	0.79	0.74	16.82**
	V5~1/V4~6	-0.54	1.07	0.97	207.47**
	V6~2/V5~7	-0.53	1.09	0.97	205.60**
	V7~3/V6~8	-0.49	1.17	0.86	41.50**
	V8~4/V7~1	-0.19	0.71	0.74	25.67**
	Combined	-0.42	1.01	0.96	106.76**

1. $V_{Path\ D}/V_{Path\ B}$, ratio of the stress wave velocity along paths D to B.
2. Stress wave velocity of path D ($V_{Path\ D}$), including from probes 1 to 5 ($V_{1\sim5}$), 2 to 6 ($V_{2\sim6}$), 3 to 7 ($V_{3\sim7}$), 4 to 8 ($V_{4\sim8}$), 5 to 1 ($V_{5\sim1}$), 6 to 2 ($V_{6\sim2}$), 7 to 3 ($V_{7\sim3}$), and 8 to 4 ($V_{8\sim4}$).
3. Stress wave velocity of path B ($V_{Path\ B}$), including from probes 2 to 8 ($V_{2\sim8}$), 1 to 3 ($V_{1\sim3}$), 2 to 4 ($V_{2\sim4}$), 3 to 5 ($V_{3\sim5}$), 4 to 6 ($V_{4\sim6}$), 5 to 7 ($V_{5\sim7}$), 6 to 8 ($V_{6\sim8}$), and 7 to 1 ($V_{7\sim1}$).

** Significant difference at $p < 0.01$.

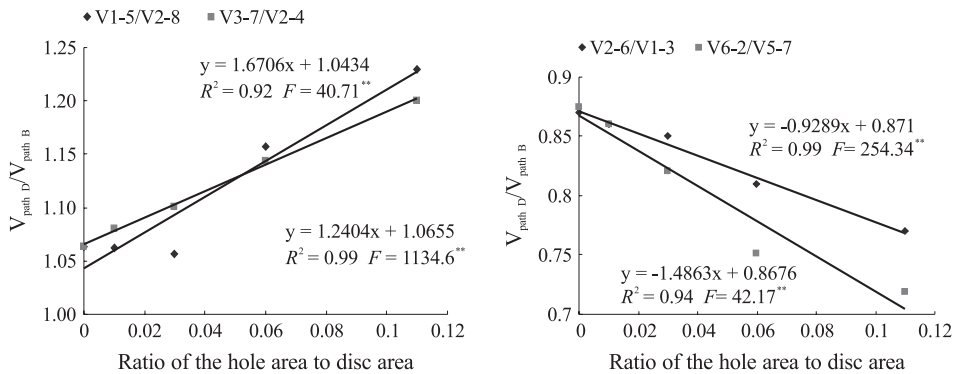

Fig. 4. Relationships between the stress wave velocity along path D to B ($V_{Path\ D}/V_{Path\ B}$) and the ratio of the hole area to disc area for detecting a defect in the side area. For a description of $V_{Path\ D}/V_{Path\ B}$, see Table 3.

Table 4 shows correlations among stress wave velocities obtained from stress wave tomography, the ratio of the hole to disc diameter, the residual disc diameter ratio, and the ratio of the hole to disc area, as analyzed by linear regression (Y = AX + B) formulae for detecting a defect in the central section. These results were significant at the 0.01 confidence level, and r^2 values of the regression analysis were 0.78~0.90.

2D tomograms for evaluating a central defect in wood discs by stress wave tomography are shown in Fig. 5. More green on the tomogram indicates a higher stress wave velocity. The highest velocity was 1500 m s^{-1}. On the contrary, more red on the tomogram

Table 4. Correlations among stress wave velocities obtained from 2D tomography, the ratio of the hole to disc diameter (RH), the residual disc diameter ratio (RR), and the ratio of the hole to disc area (HD), as analyzed by linear regression formulae (Y = AX + B) for detecting a hole in the central section

Y	X	Regression equations	R^2	F values
Stress wave velocity obtained from 2D tomography	RH	Y = -76.24x + 1249.5	0.78	25.18**
	RR	Y = 76.06x + 1173.4	0.78	25.11**
	HD	Y = -119.23x + 1242.7	0.90	64.43**

** Significant difference at $p < 0.01$.

indicates a lower stress wave velocity. The lowest velocity was 360 m s^{-1}. As shown in Fig. 5, the color of the tomograms gradually changed from green to red as the hole was gradually enlarged from 0 to 240 mm in diameter at intervals of 30 mm. Color differences between the central area and its surrounding area were detectable when the hole diameter was 60 mm (the ratio of the hole to disc area was 2.3%). Divos and Divos (2005) reported that the resolution of an acoustic tomographic system is 2.5% (with 8 channels, the velocity difference is 100 m s^{-1}). In this study, 2D tomograms for evaluating a central defect in wood discs by stress wave tomography also revealed that a slight yellow and red area in the central area of the disc was observed with a hole diameter of 60 mm.

2D tomograms of side defect evaluation of discs by stress wave tomography are shown in Fig. 6. As shown in Fig. 6, more green in the tomogram indicates a higher stress wave velocity. The highest velocity was 1400 m s^{-1}. On the contrary, more pink (from yellow to red to pink) in the tomogram indicates a lower stress wave velocity. The lowest velocity was 800 m s^{-1}. The color of the tomograms gradually changed from green to yellow and red as the diameter of hole gradually increased. The yellow and red area in the upper right part of tomogram was detectable when the diameter of the hole was 60 mm.

Relationship between stress wave velocities and wood density

In order to further evaluate wood density

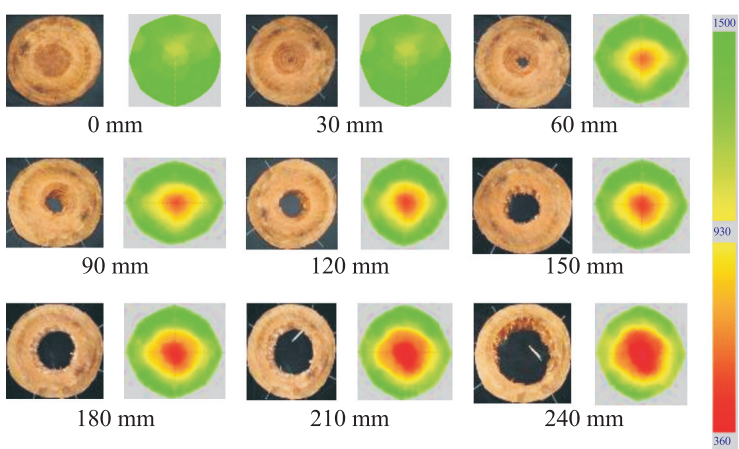

Fig. 5. Discs (left) and 2D tomographic images (right) of various central hole sizes by the Arbotom stress wave technique.

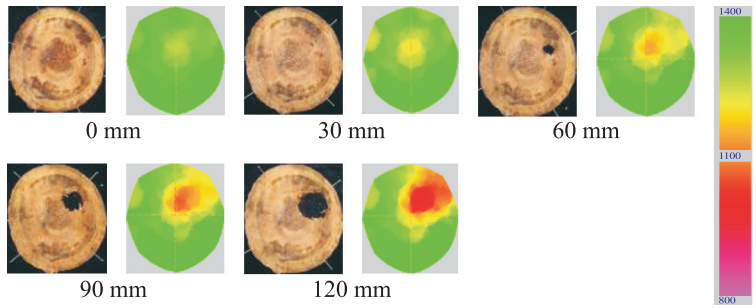

Fig. 6. Discs (left) and 2D tomographic images (right) of various side hole sizes by the Arbotom stress wave technique.

variations, a disc of a visually solid camphor tree was adopted, and the 2D tomograms were first converted into 256 gray shades using the Arbotom 2D software. The stress wave velocity at each pixel of the tomogram was then calculated using our custom-made program, based on the linear relationship between the grayscale value and the velocity, and was exported to a Microsoft Excel file for further analyses (Fig. 7). The same air-dried

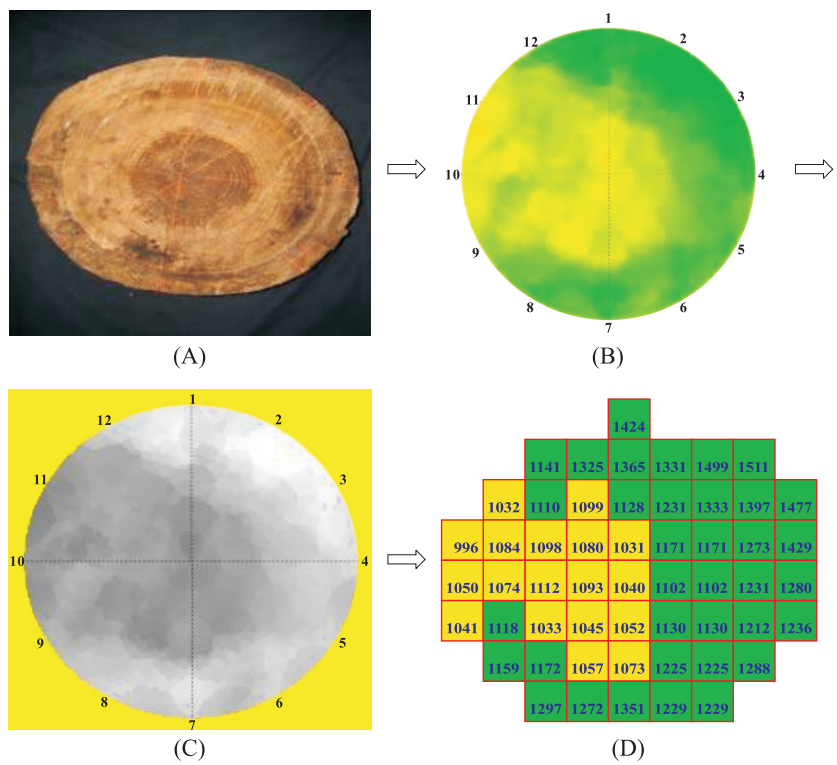

Fig. 7. Flow chart (from A to D) for analyzing the relationship between the stress wave velocity and wood density. (A) Photograph of a disc (12 probs in circumference). (B) 2D stress wave tomogram (color, red-yellow-green). (C) 2D stress wave tomogram (grayscale). (D) Stress wave velocity in cross-section of disc by 2D tomography and Borland C++ builder.

disc was detected by the stress wave system. The wood density of the small specimen and stress wave velocity of the disc from the corresponding position of 2D tomographic image were calculated and estimated. The relationship between the stress wave velocity and wood density could be represented by a positive linear regression formula (Fig. 8, r^2 = 0.49**). The result showed that the simulated variant wood density of the central part of the disc by fungi could be detected based on this experiment.

Effects of MCs on the stress wave velocity

The relationships between stress wave velocity and MCs for paths A, B, C, and D could be represented by negative linear regression formulae (Fig. 9). The determination coefficients were highly significant at the 0.01 level, as indicated by the *F* test. Therefore, the stress wave velocities were affected by different MCs (from 90 to 45%). The stress

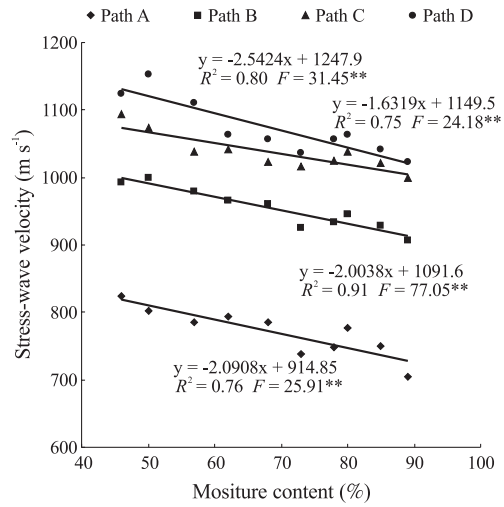

Fig. 9. Relationship between the stress wave velocity and moisture content in the different measurement directions.

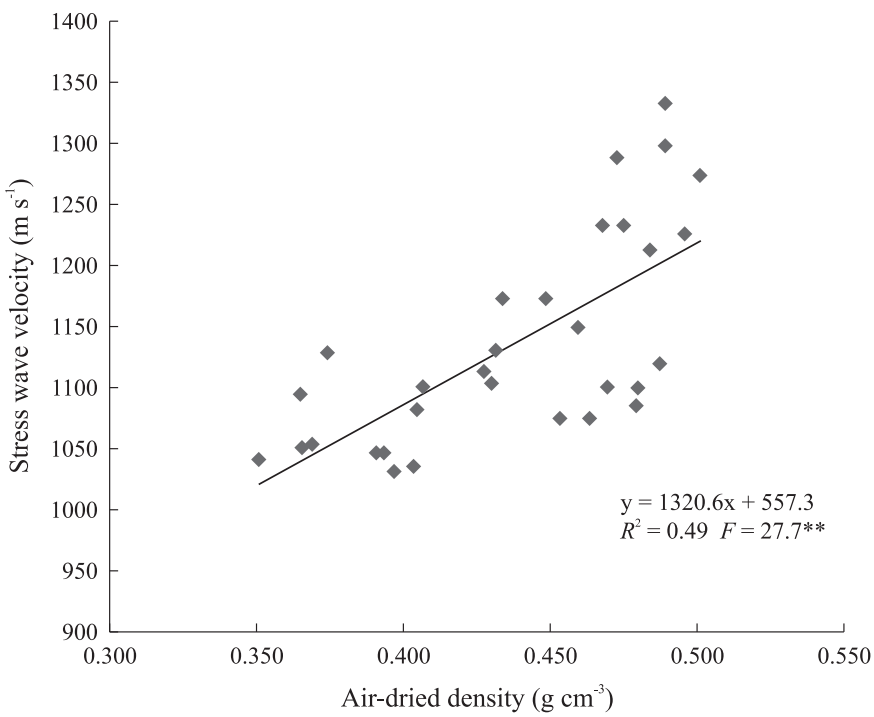

Fig. 8. Relationship between the stress wave velocity and wood density from the measurements of the 2D stress wave tomogram.

wave velocity in 4 different detected directions showed the following trend: path D > path C > path B > path A. Clearly, the stress wave velocity in the virtual radial direction (path D) was faster than that in the virtual tangential direction (path B). This is similar to the results reported by Wang et al. (2002). Therefore, when applied to living trees, the detected stress wave velocity has to take into account the MC to achieve a better interpretation of the 2D image.

CONCLUSIONS

The purpose of this study was to evaluate artificial holes in trees using a stress wave tomographic technique. In order to simulate different types of defects, a hole was chiseled in the central and side areas of trunk cross-sections, and then the stress wave velocities were measured in multiple directions and analyzed using the Arbotom system. Results showed that the residual disc diameter ratio increased with an increasing stress wave velocity and decreasing reduction in the corresponding stress wave velocity in the virtual radial direction (coefficient of determination, $r^2 = 0.96$**). The stress wave velocity ratios in the path D to path B directions ($V_{Path\ D}/V_{Path\ B}$) decreased with an increasing ratio of the center hole to disc area. However, the $V_{Path\ D}/V_{Path\ B}$ values became more diverse for specimens with a hole chiseled in the side area as the ratio of the hole to disc area increased.

Differences in the mapped colors and stress wave velocities between the hole area and its surrounding area were obvious, and when the ratio of the hole area to the cross-sectional area exceeded 2.3%, the hole was detectable by Arbotom tomography.

The stress wave velocity tended to increase with increasing wood density of the transverse section. When moisture contents of tree were above the fiber saturation point, stress wave velocity values tended to decrease with increasing moisture contents using this tomographic image technique.

ACKNOWLEDGEMENTS

The authors wish to thank the Architecture and Building Research Institute, Ministry of the Interior and Taiwan Forestry Research Institute for financial support.

LITERATURE CITED

Anonymous. 2005. Arbotom manual – three-dimensional impulse tomography for examination of trees and timber. Rinntech, Heidelberg, Germany: RINNTECH. 33 p.

Bauer C, Kilbertus G, Bucur V. 1991. Technique ultrasonore de caractérisation du degré d'altération des bois de hêtre et de pin soumis à l'attaque de differents champignons. Holzforschung 45(1):41-6.

Bethge K, Mattheck C, Hunger E. 1996. Equipment for detection and evaluation of incipient decay in trees. Arboricult J 20(1):13-37.

Biagi E, Gatteschi G, Masotti L, Zanini A. 1994. Tomografia ad ultrasuoni per la caratterizzazione difettologica del legno. Alta frequenza – rivista dielettronica 6(2):48-57.

Bucur V. 1995. Acoustics of wood. Boca Raton, FL: CRC Press. 286 p.

Bucur V. 2003. Techniques for high resolution imaging of wood structure: a review. Meas Sci Technol 14:R91-8.

Comino E, Socco V, Martinis R, Nicolotti G, Sambuelli L. 2000. Ultrasonic tomography for wood decay diagnosis. In Backhaus GF, Balder H, Idczak E, editors. International Symposium on Plant Health in Urban Horticulture; 2000 May 22-25; Braunschweig, Germany: Parey Buchverlag. 279 p.

Deflorio G, Fink S, Schwarze FWM. 2008. Detection of incipient decay in tree stems with sonic tomography after wounding and fungal inoculation. Wood Sci Technol 42:117-32.

Divos F, Divos P. 2005. Resolution of stress wave based acoustic tomography. Proceedings of the 14th International Symposium on Nondestructive Testing of Wood; 2005 May 2-4; University of Applied Sciences; Eberswalde, Germany: Shaker Verlag. ISBN 3832239499. p 16-20.

Gilbert E, Smiley ET. 2004. Picus sonic tomography for the quantification of decay in white oak (*Quercus alba*) and hickory (*Carya* spp.). J Arboriculture 30(5):277-81.

Hoyle RJ, Pellerin RF. 1978. Stress wave inspection of a wood structure. Proceedings of 4th Symposium on Nondestructive Testing of Wood; Pullman, WA: Washington State Univ. p 33-45.

Huang YS, Chen SS, Chang CC, Ho YM. 1997. Application of ultrasound for detection wood decay on the standing tree of *Casuarina equisetifolia*. Q J Chin For 30(4):445-50.

Lin CJ, Chiu CM, Wang SY. 2000. Application of ultrasound in detecting wood decay in squirrel-damaged standing trees of Luanta China fir. Taiwan For Sci 15(2):267-79.

Lin CJ, et al. 2008. Application of an ultrasonic tomographic technique for detecting defects in standing trees. Int Biodeter Biodegr 62(4):434-41.

Mattheck CG, Bethge KA. 1993. Detection of decay in trees with the Metriguard Stress Wave Timer. J Arboricult 19(6):374-8.

McCracken FI. 1985. Using sound to detect decay in standing hardwood trees. Proceedings of 5th International Symposium on Nondestructive Testing of Wood; 1985 Sep 9-11; Pullman, WA: Washington State Univ. p 281-7.

Nicolotti G, Socco LV, Martinis R, Godio A, Sambuelli L. 2003. Application and comparison of three tomographic techniques for detection of decay in trees. Arboricult J. 29(2):66-78.

Ross RJ, Pellerin RF. 1994. Nondestructive testing for assessing wood members in structures: a review. Gen Tech Rep FPL-GTR-70. Madison, WI: US Department of Agriculture, Forest Service, Forest Products Laboratory. 40 p.

Rust S, Gocke L. 2000. PICUS sonic tomography – a new device for nondestructive timber testing. In: Backhaus GF, Balder H, Idczak E, editors. International Symposium on Plant Health in Urban Horticulture; 2000 May 22-25; Braunschweig, Germany: Argus Electronic. 300 p.

Schad KC, Schmoldt DL, Ross RJ. 1996. Nondestructive methods for detecting defects in softwood logs. General Technical Report FPL-RP-546. Madison, WI: Forest Products Laboratory, Forest Service, US Department of Agriculture. p 1-13.

Stewart RR. 1991. Exploration of seismic tomography: fundamentals. Society of Exploration Geophysicists course notes. Tulsa, OK: Society of Exploration Geophysicists. 190 p.

Tomikawa Y, Iwase Y, Arita K, Yamada H. 1990. Nondestructive inspection of wooden poles using ultrasonic computed tomography. IEEE Transact UFFC 33(4):354-8.

Wang SY, Chiu CM, Lin CJ. 2002. Variations in ultrasound and dynamic young's modulus with moisture content for Taiwania plantation lumber. Wood Fiber Sci 34(3):370-81.

Wang X, Allison RB. 2008. Decay detection in red oak trees using a combination of visual inspection, acoustic testing, and resistance microdrilling. Arboricult Urban For 34(1):1-4.

Wang X, Allison RB, Wang L, Ross RJ. 2007. Acoustic tomography for decay detection in red oak trees. Research Paper FPL-RP-642. Madison, WI: Forest Products Laboratory, Forest Service, US Department of Agriculture. p 1-7.

Wang X, Wiedenbeck J, Liang S. 2009.

Acoustic tomography for decay detection in black cherry trees. Wood Fiber Sci 41(2):127-37.

Wilcox WW. 1988. Detection of early stages of wood decay with ultrasonic pulse velocity. For Prod J 38(5):68-73.

Yamamoto K, Sulaiman O, Hashim R. 1998. Nondestructive detection of heart rot on *Acacia mangium* trees in Malaysia. For Prod J 48(3): 83-6.